Journal of Sciences, Islamic Republic of Iran 23(4): 319-335 (2012) http://jsciences.ut.ac.ir
University of Tehran, ISSN 1016-1104

The Origin of Co-Magmatic Andesite Enclaves in the Rabor Miocene Pyroxene Andesites, SE Kerman, Iran: Insights from Textural and Mineralogical Composition

S. Dargahi,[1,*] M. Arvin,[1,2] Y. Pan,[2] and A. Babaei[3]

[1]*Department of Geology, Faculty of Sciences, Shahid Bahonar University of Kerman, Kerman, Islamic Republic of Iran*
[2]*Department of Geological Sciences, University of Saskatchewan, Saskatoon, Canada*
[3]*Biological, Geological and Environmental Sciences, Cleveland State University, Cleveland, U.S.*

Received: 14 February 2011 / Revised: 24 September 2012 / Accepted: 25 December 2012

Abstract

The Miocene pyroxene andesite lava flows are exposed in southeastern edge of Urumieh Dokhtar Magmatic assemblage in Iran. The hypocrystalline andesite in parts contain conspicuous co-magmatic igneous enclaves which are dark grey and occur mostly as spherical and occasionally as ribbon shapes with some showing chilled margins. Petrographic study shows that the ribbon type enclaves have been formed by merging of rounded blobs. Mineralogically the enclaves consist of plagioclase, clinopyroxene, orthopyroxene and magnetite as phenocrysts and microphenocrysts in a glassy microlitic groundmass of the same minerals. The host andesite contains the same mineral assemblage, but with high amount of glassy groundmass. The plagioclase shows a relatively large range of anorthite content (An_{43-91}), whereas pyroxenes generally show a uniform chemical composition and are classified mainly as hypersthene ($En_{59.67}$ to $En_{73.30}$) and augite ($Wo_{40.88-46.00}$, $Fs_{11.08-17.07}$, $En_{36.69-47.85}$). Enclaves are cogenetic with the host andesites and reveal the existence of disequlibrium crystallization in the magma chamber. The enclaves are resulted from a magmatic emulsion with suspended droplets of one magma in another. The rounded enclaves are likely to represent quenched blebs of intruding new andesite magma with higher liquidus that have been incorporated into the host andesitic magma in a liquid or near liquid state. Their small sizes reflect a small viscosity contrast and some turbulence during mixing. The intrusion of fresh magma also resulted convection in the magma chamber which along with the temperature differences has permitted buoyant uprising of enclaves and incorporating some of the phenocrysts from the host andesitic magma.

Keywords: Pyroxene andesite; Enclaves; Rabor; Disequilibrium; Magma mixing

Introduction

Andesites represent abundant rock types in many subduction zones and are regarded to play an important role in the formation and evolution of the continental crust at convergent margins [48,38]. Their formations

* Corresponding author: Tel: +98(341)3202230, Fax: +98(341)3222035, E-mail: s.dargahi@uk.ac.ir

are dominated by mixing of iron and magnesium rich (mafic) magmas and silicate rich (felsic) magmas [53, 52 and 38]. Many porphyritic andesites display a range of disequilibrium features such as: coexisting of minerals which are not in equilibrium with each other and with their enclosed matrix, complex zoning patterns, resorption surfaces and embayed structure [19, 6 and 52]. All these represent a complex rock history but progresses in detailed petrographic studies of phenocrysts have played an important role in andesite petrogenesis [54, 39, 45, 32, 15, 38 and 58]. The mineralogical study has this advantage that there is no longer a need to use the restraint factor of chemical analyses as a representative of liquid composition in order to assess the andesite petrogenesis. However, interpretation of obtained mineralogical data (such as geothermometry, geobaraometry, and element partitioning) can be tricky under conditions that have been drifted from equilibrium [32]. On the other hand, the enclaves are interpreted to form by mingling- in the liquid state- of coexisting magmas with strongly contrasting physical properties [22, 7, 59, 63, 40, 63 and 14]. Also, the types and morphologies of enclaves in the host lavas preserve information on the style and dynamics of the mingling magmas [14]. The presence of mafic magmatic enclaves, or inclusions, in many intermediate to silicic volcanic rocks are interpreted as the products of magma replenishment and mixing eventsbetween two at least partially molten magmas [8, 7, 17, 46, 18, 43]. Groundmass texture and crystal morphologies observed in the enclaves are interprted as an indication of the degree of undercooling between the enclaves and the host enclaves, which in turn a function of the thermal and compositional contrast between the inclusions and the host magma [7, 18]. Study of the inclusions constrains their origin as well as the origin of the host andesitic lava flows [31].

The purpose of this paper is to point out detailed morphological characteristics and petrography of both the andesite enclaves and their host andesitic lava flows. Integrating this with mineral chemistry; the paper attempt to establish the crystallization conditions and processes that led into the formation of enclaves. The results may contribute as an insight into the magma chamber processes.

Materials and Methods

Geological Setting

The study area is located within the southeastern edge of the Dehaj-Sarduiyeh volcanic belt [21], a southeastern part of the Urumieh-Dokhtar Magmatic

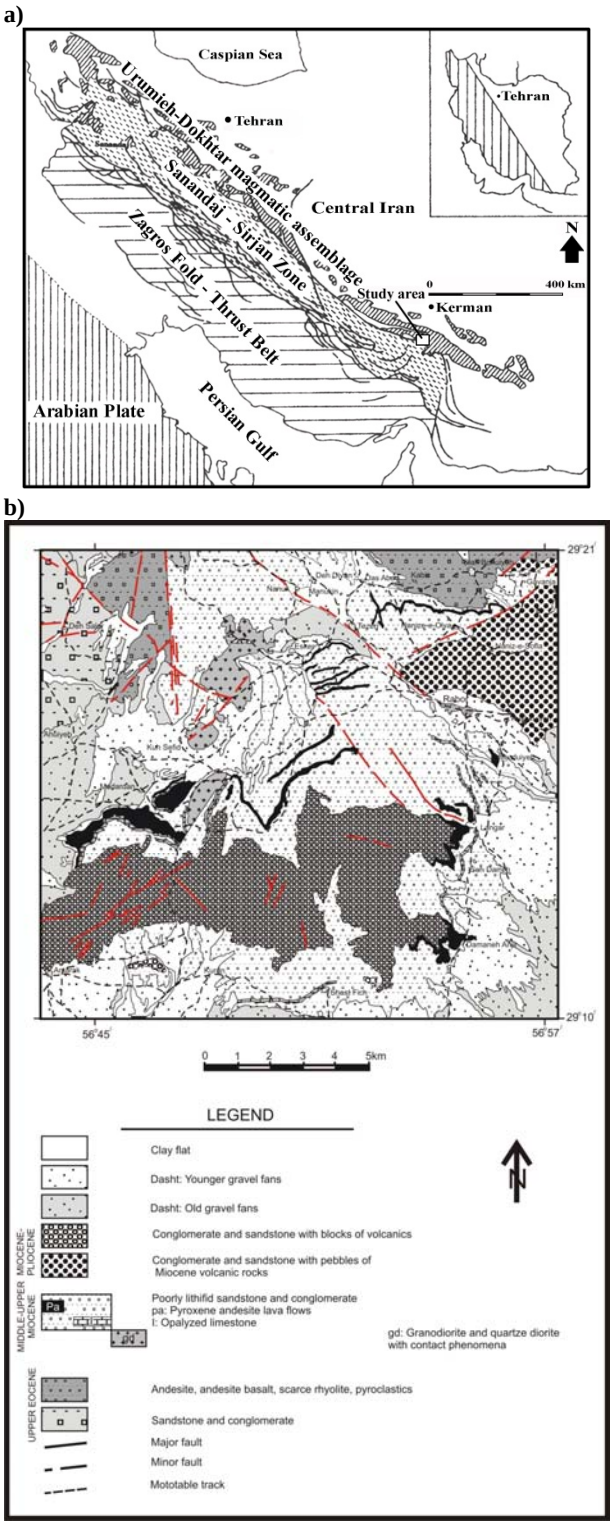

Figure 1. a. Simplified geological map of Iran illustrating major lithotectonic units in the Zagros orogenic belt and the study area. b. Simplified geological map of the study area, southwest of Kerman (modified from the Geological Map of Iran, 100,000 Series, Sheet 7348, Baft, [62].

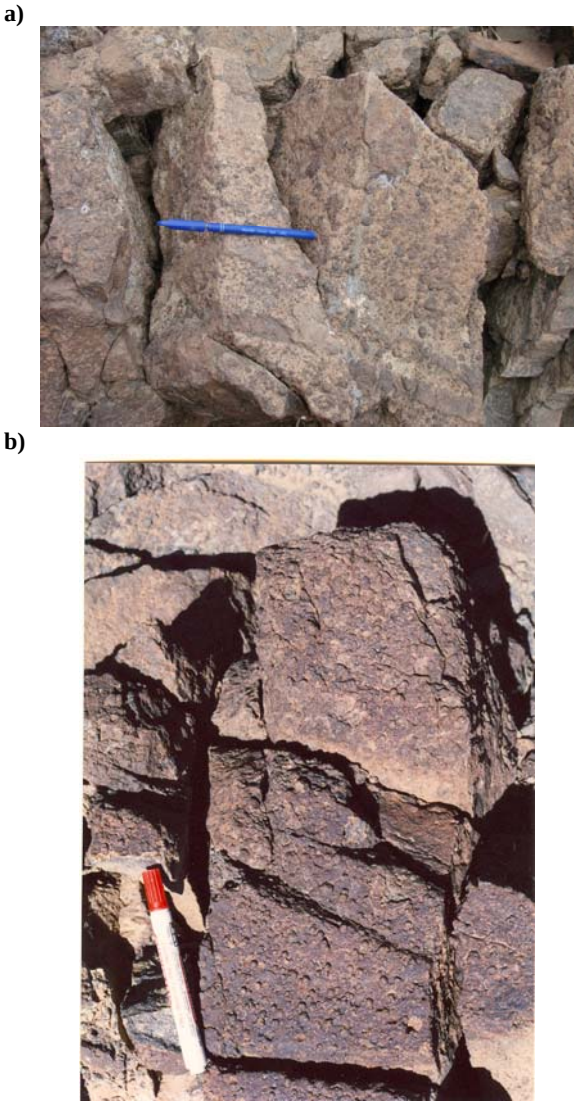

Figure 2. a. Rabor andesite showing both ribbon and spherical to ellipsoidal shape andesitic enclaves. Notice the latter type coalescence (leading to formation of ribbon enclaves) and its detachment from ribbon enclave (leading to its disintegration). b. Rabor andesite showing swarms of spherical to ellipsoidal shape enclaves.

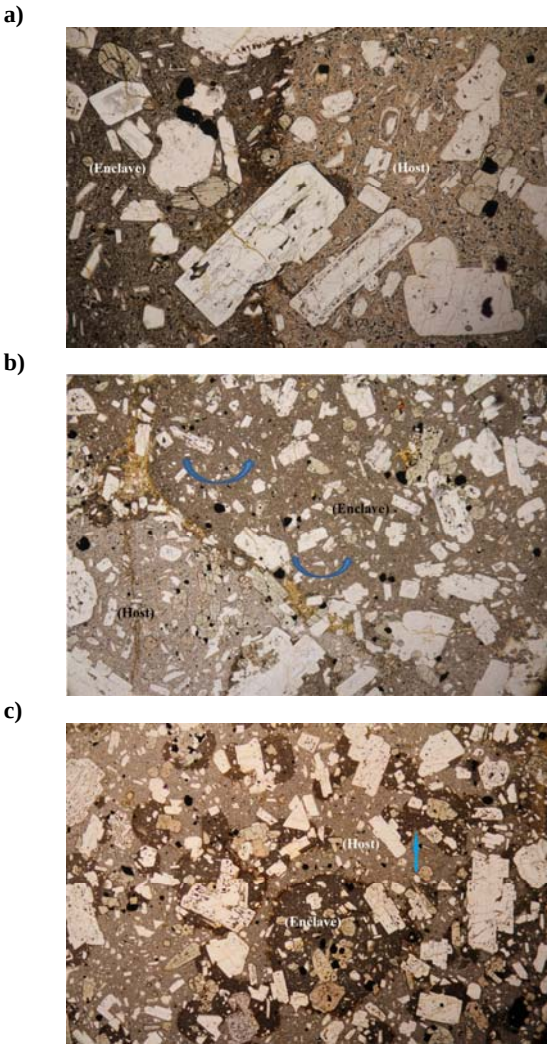

Figure 3. Photomicrographs (in plane-polarized light with field of view is 10 mm across) showing andesitic enclaves in the Rabor andesitic host rock. (a, b) Ribbon type. (c) Spheroidal to ellipsoidal type. In all three figures notice crystal capturing of entrained crystals originally presented in the host andesitic magma at the time of mingling. Notice the merging of enclaves in figure 3c (arrow) and anti-clockwise rotation in figure 3b (curved arrows).

Assemblage (UDMA) of Zagros orogenic belt of Iran [e.g., 26, 35, 10, 3, 5 and 57] (Fig. 1a). The Zagros orogenic belt of Iran belongs to the extensive Alpine-Himalayan orogenic system, formed as a result of collision between the Arabian and Eurasian plates during Cenozoic times and constitutes a morphological barrier (with some peaks exceeding 4000 m) separating the Arabian platform from the large plateaux of central Iran [42]. The Zagros orogen and the Iranian plateau preserve a record of the long-standing convergence history between Eurasia and Arabia across the Neo-Tethys, from subduction/obduction processes to present-day collision (from 150 to 0 Ma) [2]. Structurally, the Zagros orogenic belt consists of three parallel NW-SE trending units (Fig. 1). 1. The Zagros fold–thrust belt (ZFTB) extends about 2000 km from Turkey in the NW to the Hormuz Strait in the SE and contains a thick and almost continuous sequence of shelf sediments deposited on the 1-2 km thick Infra-Camberian Hormoz salt formation. These sediments, of Paleozoic to Late

Tertiary age, are believed to be separated from the Precambrian metamorphic basement by the Hormoz salt layer [4, 1]. 2. The Sanandaj-Sirjan zone (SSZ; [65]) is made of mainly Jurassic, interbedded phyllites and metavolcanics showing a moderate metamorphic imprint except close to large-scale Mesozoic calc-alkaline plutons. These metamorphic rocks are unconformably overlain by the Barremo–Aptian Orbitolina limestones, typical of Central Iran sedimentation [65]. During most of the second half of the Mesozoic, the SSZ represented an active Andean-like margin whose calc–alkaline magmatic activity progressively shifted northward [9, 56]. 3. The Urumieh-Dokhtar volcanic zone of Schroder [55] or the Urumieh-Dokhtar magmatic assemblage (UDMA) of Alavi [5] is a 150 km wide magmatic assemblage. This magmatic assemblage has been interpreted to be a subduction related Andean type magmatic arc that has been active from the Late Jurassic to present [9 and 10]. The UDMA is composed of voluminous tholeiitic, calc-alkaline, and K-rich alkaline intrusive and extrusive rocks (with associated pyroclastic and volcaniclastic successions) along the active margin of the Iranian plates. The oldest rocks in the UDMA are calc-alkaline intrusive rocks, which cut across Upper Jurassic formations and are overlain nonconformably by Lower Cretaceous fossiliferous limestone. The youngest rocks in the UDMA consist of lava flows and pyroclastics that belong to Pliocene to Quaternary volcanic cones of alkaline and calc-alkaline composition [9].

Field Geology

The Study area lies in N-NW and S-SW of Rabor, 140 km southwest of Kerman, in southeastern part of the Urumieh-Dokhtar Magmatic Assemblage (UDMA) Iran (Fig. 1b) [21]. The sequence consists of poorly exposed Miocene sequence of weakly lithified sandstones and conglomerates. In is lower parts the sequence contains opalitized limestones with poorly preserved faunas, pointing to a middle-upper Miocene agae. The whole sequenec overlay unconformably on the middle Miocene Upper Red formation. In the sequence occur dispersed exposures of massive micro-porphyritic pyroxene andesite lava flows, in average 100 meter thick, in the lower part of the sequence. The contact between the opalitized limestone's and pyroxene andesite lava flows is depositional. In some localities at the top of andesite lava flows conspicuous dark grey enclaves can be observed which their magmatic origin is particularly clear. However, their abundances do not vary systematically with their positions within lava flows. They are occurring mostly as spherical (like varioles) and occasionally as thin ribbons and rarely as angular shape (Fig. 2a). The ribbon enclaves have an average thickness of 1-4 cm whereas the spherical shape enclaves range from 0.5 to 6 cm in diameter and dispersed throughout the host andesite (Fig. 2a). They have sharply defined, smooth contacts with the host andesitic magma (Fig. 2a) and some showing chilled margins. Where the two types of enclaves are seen together (Fig. 2a), the coalescence of spherical enclaves which leads to the formation of ribbon enclaves and their detachment from ribbon enclaves which leads to their disintegration is quite noticeable. Locally, spherical enclaves occur in swarms of anomalously high concentration relative to the surrounding host andesitic rock (Fig. 2b). The hosted pyroxene andesites consist of plagioclase and pyroxene phenocrystes setting in a glassy matrix of microlitic plagioclase, pyroxene and opaque. The enclaves are more crystallized and have the same mineralogy of the host rock with less glassy matrix.

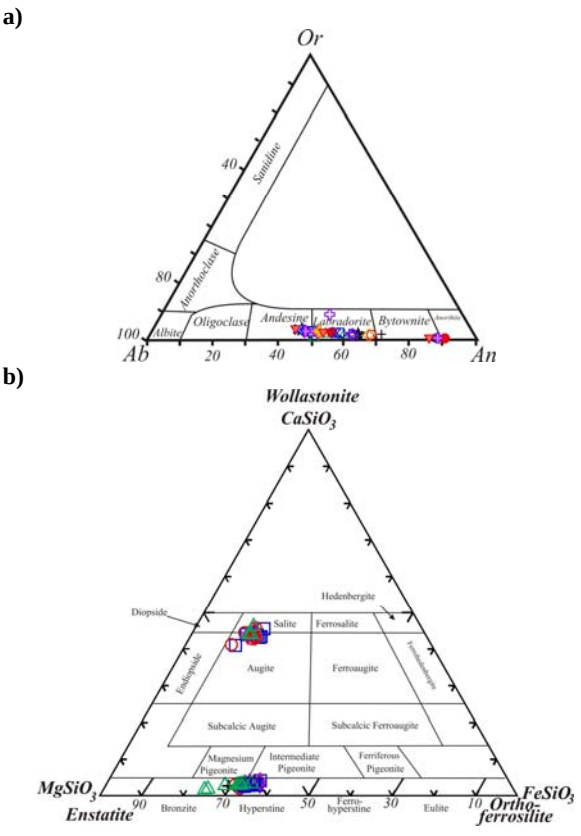

Figure 4. a. Plagioclase phenocrysts and microphenocrysts core/rim and microlitic groundmass compositions as calculated from microprobe analysis. b. Representative of pyroxene compositions plotted as mole% of the simple quadrilateral components. Symboles: S-11= Circle, S-11-1= Quadrangle, S11-2= Diamond, S-14= +, S-25= Triangle.

Table 1. Representative electron microprobe (oxide in wt%) analyses of plagioclase from Rabor andesites

Sample	S-11-1					S-11-2								
Grain	P1			P2		P3			P4	P5	P6	P7	P8	
Position	(Enclave)			(Host)		(Enclave)			(Enclave)	(Enclave)	(Enclave)	(Enclave)	(Enclave)	
	Edge	Middle	Core	Edge	Core	Edge	Middle	Core	Microlite	Microlite	Microlite	Microlite	Edge	Core
Type	1			2		1			3	3	3	3	2	
SiO_2	55.88	53.38	54.96	55.88	53.75	52.43	56.41	52.13	54.69	54.4	55.87	50.41	54.42	45.43
TiO_2	0	0.0335	0.0332	0.0363	0.0538	0.0281	0.0294	0.0223	0	1.3235	0.0354	0.0431	0.0326	0.0467
Al_2O_3	26.3	28.79	27.29	27.08	28.12	28.21	26.42	28.96	26.43	26.86	26.32	30.03	27.93	33.41
Fe_2O_3	0.7087	0.4527	0.4507	0.4095	0.4243	0.4703	0.3133	0.427	0.4057	0.3406	0	0.4285	0.46	0.3637
CaO	9.74	12.07	10.98	10.16	11.43	12.45	10.09	12.98	10.38	10.73	9.82	14.29	11.73	18.88
SrO	0.4093	0	0	0	0	0	0	0	0	0.1019	0	0	0	0
BaO	0	0	0	0.0726	0.2227	0.1146	0.1072	0	0.0057	0	0	0.196	0.1796	0
Na_2O	5.1	4.35	4.99	5.42	4.71	4.75	5.8	4.11	5.52	5.36	5.8	3.54	4.93	1.0064
K_2O	0.0312	0.2333	0.2932	0.3997	0.2554	0.3416	0.443	0.213	0.4363	0.3391	0.474	0.183	0.3479	0.0284
Total	98.16	99.32	99.00	99.45	98.97	98.80	99.61	98.84	97.87	99.45	98.33	99.12	100.03	99.17
Si	10.236	9.732	10.02	10.127	9.838	9.669	10.217	9.587	10.097	9.912	10.229	9.303	9.87	8.471
Ti	0	0.0046	0.0046	0.0049	0.0074	0.0039	0.004	0.0031	0	0.1814	0.0049	0.006	0.0044	0.0065
Al	5.678	6.187	5.865	5.784	6.065	6.131	5.639	6.276	5.751	5.768	5.68	6.532	5.971	7.342
Fe	0.0977	0.0621	0.0618	0.0559	0.0584	0.0653	0.0427	0.0591	0.0564	0.0467	0	0.0595	0.0628	0.051
Ca	1.9114	2.3583	2.1455	1.9723	2.2422	2.4607	1.9581	2.5587	2.0533	2.0951	1.9262	2.8252	2.28	3.771
Sr	0.0435	0	0	0	0	0	0	0	0	0.0108	0	0	0	0
Ba	0	0	0	0.0052	0.016	0.0083	0.0076	0	0.0004	0	0	0.0142	0.0128	0
Na	1.811	1.5376	1.7637	1.9044	1.6721	1.6996	2.0358	1.4668	1.9776	1.8926	2.0606	1.2666	1.7328	0.3638
K	0.0073	0.0543	0.0682	0.0924	0.0596	0.0804	0.1024	0.05	0.1028	0.0788	0.1107	0.0431	0.0805	0.0068
O	32	32	32	32	32	32	32	32	32	32	32	32	32	32
CatTot	19.785	19.935	19.928	19.946	19.959	20.119	20.007	20.001	20.039	19.985	20.012	20.05	20.015	20.012
Total	51.785	51.935	51.928	51.946	51.959	52.119	52.007	52.001	52.039	51.985	52.012	52.05	52.015	52.012
Ab	48.5561	38.9246	44.3430	47.9178	41.9083	40	49.6064	35.9906	47.8362	46.5412	50.2892	30.5271	42.2006	8.7840
An	51.2480	59.7007	53.9422	49.626	56.1969	57.9124	47.7131	62.7824	49.6674	51.5209	47.0091	68.0918	55.5271	91.0517
Or	0.1957	1.3746	1.7146	2.45577	1.8947	2.0875	2.6803	1.2268	2.49631	1.9377	2.7016	1.3810	2.2722	0.1641

Analytical Technique

Electron microprobe analyses were performed on plagioclase, pyroxene and glassy matrix of both enclaves and host andesitic rocks in Department of Geological Sciences at University of Saskatchewan on a JEOL JXA-8600 Superprobe equipped with three automated wavelength-dispersion and one energy-dispersion spectrometers. Results were corrected with a ZAF matrix correction program. Run conditions were 15 kV accelerating voltage, beam current of 10 nA and beam diameter of 5 µm. Collection times varied from 20 to 60 s perelement. Instrument calibration was performed using cobalt metal and natural mineral standards.

Petrography and Mineralogy

The pyroxene andesite host rocks are dark and brownish red on fresh and altered surfaces respectively and contain many enclaves. The host andesite has hypocrystalline porphyritic to glomeroporphyritic textures and is relatively highly crystalline, consisting of 40-45 vol% phenocrysts (>1mm) and microphenocrysts (0.01-0.07 mm) of plagioclase, orthopyroxene, clinopyroxene and subordinate Fe-oxides sitting in a glassy microlitic (<0.01mm) groundmass of the same mineralogy (Fig. 3a). Plagioclase phenocrysts display disequilibrium phenomenates such as sieved textures, zoning and reaction rims. Apatite and magnetite are the accessory minerals. Although majority of the Rabor pyroxene andesites are macroscopically homogeneous,

Table 1. Continue

Sample	S-11										S-25				
Grain	P9				P10			P11			P12	P13			
Position	(Enclave)				(Enclave)			(Host)			(Enclave)	(Enclave)			
	Edge	Middle	Middle	Core	Edge	Middle	Core	Core	Middle	Edge	Microlite	Core	Middle	Middle	Edge
Type	1				1			2			3	2			
SiO_2	50.98	55.12	46.37	50.05	52.25	57.08	46.58	52.38	52.56	57.3	57.19	55.61	52.05	52.35	53.74
TiO_2	0.0274	0.0436	0	0	0.0294	0.0492	0.0199	0.0242	0.0171	0.0029	0.023	0.0174	0.0306	0.0381	0.2678
Al_2O_3	29.98	27	33.11	30.17	29.25	26.51	32.69	29.28	29.11	26.22	26.31	26.99	28.12	28.91	27.99
Fe_2O_3	0.6038	0.4424	0.38	0.4822	0.6198	0.3842	0.3344	0.3451	0.4194	0.3733	0.3983	0.4522	0.4551	0.4198	0.4165
CaO	14.55	11.4	17.53	15.57	13.81	9.84	18.49	13.5	13.04	9.99	9.86	10.62	12.98	12.93	11.72
SrO	0	0	0	0	0	0	0	0	0	0	0	0	0	0	0
BaO	0	0	0.0356	0	0.089	0	0.0694	0.1283	0	0	0.2014	0.1034	0	0	0
Na_2O	3.1	5.27	1.32	3.05	4.06	5.95	1.3437	4.02	4.21	6.11	6.02	5.5	4.29	4.12	4.96
K_2O	0.2839	0	0.0405	0	0.2704	0.4864	0	0.2539	0.2332	0.574	0.5669	0.4413	0.2837	0.26	1.6317
Total	99.52	99.28	98.79	99.33	100.37	100.30	99.54	99.94	99.59	100.57	100.57	99.74	98.21	99.03	100.73
Si	9.351	10.029	8.637	9.225	9.506	10.252	8.641	9.549	9.596	10.28	10.269	10.082	9.649	9.608	9.757
Ti	0.0038	0.006	0	0	0.004	0.0066	0.0028	0.0033	0.0024	0.0004	0.0031	0.0024	0.0043	0.0053	0.0366
Al	6.481	5.79	7.268	6.554	6.271	5.612	7.148	6.292	6.263	5.544	5.568	5.767	6.144	6.254	5.99
Fe	0.0833	0.0606	0.0533	0.0669	0.0849	0.0519	0.0467	0.0473	0.0576	0.0504	0.0538	0.0617	0.0635	0.058	0.0569
Ca	2.8596	2.2223	3.499	3.075	2.6926	1.8942	3.674	2.6366	2.551	1.9197	1.8968	2.0627	2.5772	2.5424	2.2797
Sr	0	0	0	0	0	0	0	0	0	0	0	0	0	0	0
Ba	0	0	0.0026	0	0.0063	0	0.005	0.0092	0	0	0.0142	0.0073	0	0	0
Na	1.1015	1.8605	0.4767	1.089	1.4308	2.0735	0.4833	1.4218	1.4888	2.1255	2.0948	1.9342	1.5416	1.4666	1.7476
K	0.0664	0	0.0096	0	0.0627	0.1114	0	0.059	0.0543	0.1313	0.1298	0.1021	0.0671	0.0609	0.3779
O	32	32	32	32	32	32	32	32	32	32	32	32	32	32	32
CatTot	19.947	19.969	19.946	20.009	20.059	20.002	20.001	20.018	20.013	20.051	20.029	20.019	20.047	19.995	20.246
Total	51.947	51.969	51.946	52.009	52.059	52.002	52.001	52.018	52.013	52.051	52.029	52.019	52.047	51.995	52.246
Ab	27.3494	45.5692	11.9536	26.1527	34.1284	50.8322	11.6113	34.4545	36.3645	50.8919	50.6528	47.1032	36.8284	36.0352	39.6713
An	71.0018	54.4307	87.7404	73.8472	64.2257	46.4367	88.2685	63.8927	62.3091	45.9643	45.8651	50.2325	61.5686	62.4683	51.7502
Or	1.6486	0	0.3059	0	1.6458	2.7309	0.1201	1.6526	1.3262	3.1437	3.4819	2.6641	1.6030	1.4963	8.5784

but enclaves with different forms are present in some parts. Apart from their shapes, the most noticeable distinction between the enclaves and the host lavas is that the enclaves are darker than the host rock in the hand specimens (Fig. 2a). The enclaves are consistently more crystalline and have a porphyritic to glomeroporphyritic texture with a cryptocrystalline microlitic less glassy matrix. The microlite for most parts consists of plagioclase and subordinate pyroxene. The enclaves show also an evidence of crystal capturing of entrained crystals, which were originally presented in the host andesitic magma at the time of mingling, and also sign of convection (Figs. 3a, b and c). Evidence of merging of spherical enclaves is visible in Figure 3c. Some enclaves have chilled margins characterized by tiny dark brownish to yellowish color rings (possibly due to glass alteration) and finer grain size at the edge. Field observation (visible magmatic enclaves) and the petrographic evidence such as sieved texture, zoning and reaction rims in plagioclase phenocrysts are indicators of disequilibrium features and magma mingling [13, 52]. The spatial distributions of magmatic enclave result in the development of an emulsion-like texture, with suspended droplets of one magma in another at higher liquidus temperature.

Petrological and geochemical data of both host rock

Table 1. Continue

Sample	S-25										
Grain	P14			P15	P16	P17	P18	P19	P20		
Position		(Enclave)		(Enclave)	(Enclave)	(Enclave)	(Enclave)	(Host)		(Host)	
	Edge	Middle	Core	Microlite	Microlite	Microlite	Microlite	In Opx	Edge	Middle	Core
Type		1		3	3	3	3	3		2	
SiO_2	56.96	56.8	46.08	53.91	57.49	51.04	55.68	54.69	55.17	57.48	47.05
TiO_2	0.039	0.0303	0	0.0209	0.0549	0.0306	0.0195	0.0314	0.0259	0.0047	0.014
Al_2O_3	26.43	26.58	33.33	28.1	25.73	29.78	27.16	27.68	27.38	25.94	32.9
Fe_2O_3	0.4424	0.4234	0.3406	0.4854	0.4618	0.4109	0.503	0.6133	0.4995	0.4844	0.4051
CaO	9.95	10.02	18.28	11.95	9.61	14.03	10.9	11.77	11.3	9.49	17.78
SrO	0	0	0	0	0	0	0	0	0	0	0
BaO	0	0.0293	0.0604	0	0.1019	0	0.0078	0.1203	0	0	0
Na_2O	5.87	5.85	1.2363	4.79	6.13	3.61	5.38	5.04	5.28	6.29	1.5359
K_2O	0.5239	0.4569	0.0233	0.3602	0.5582	0.2189	0.4637	0.4132	0.4307	0.6655	0.0664
Total	100.21	100.19	99.35	99.61	100.13	99.12	100.11	100.37	100.08	100.36	99.75
Si	10.247	10.221	8.558	9.816	10.352	9.391	10.057	9.895	9.984	10.329	8.686
Ti	0.0053	0.0041	0	0.0029	0.0074	0.0042	0.0026	0.0043	0.0035	0.0006	0.0019
Al	5.604	5.637	7.297	6.03	5.461	6.459	5.782	5.903	5.839	5.495	7.159
Fe	0.0599	0.0573	0.0476	0.0665	0.0626	0.0569	0.0684	0.0835	0.068	0.0655	0.0563
Ca	1.9169	1.9329	3.637	2.3307	1.8533	2.7656	2.1098	2.2818	2.1899	1.8276	3.518
Sr	0	0	0	0	0	0	0	0	0	0	0
Ba	0	0.0021	0.0044	0	0.0072	0	0.0006	0.0085	0	0	0
Na	2.0477	2.0402	0.4452	1.6918	2.1414	1.2881	1.8825	1.7697	1.8509	2.1911	0.5498
K	0.1202	0.1049	0.0055	0.0837	0.1282	0.0514	0.1068	0.0954	0.0994	0.1526	0.0156
O	32	32	32	32	32	32	32	32	32	32	32
CatTot	20	20	19.995	20.021	20.013	20.016	20.01	20.041	20.034	20.062	19.987
Total	52	52	51.995	52.021	52.013	52.016	52.01	52.041	52.034	52.062	51.987
Ab	50.1297	50.0036	10.8795	41.2011	51.8486	31.3780	45.9179	42.5879	44.7055	52.5279	13.4642
An	46.9276	47.3738	88.8785	56.7605	44.8730	67.3698	51.4623	54.9116	52.8935	43.8136	86.1537
Or	2.9426	2.6224	0.2419	2.0383	3.2783	1.2521	2.6197	2.5003	2.4008	3.6583	0.3820

and enclaves confirm their similarities. Composition of mineral phases in the andesite and the enclaves overlap each other. The overall impression is that the enclaves derive from similar host rock magma pulses and have been variably dispersed throughout the host andesitic magma body.

Plagioclase

Plagioclases are ubiquitous and the most abundant mineral phase, accounting for 50-55 vol% of the rock samples. The plagioclase compositions (Table 1) are shown in Fig. 4a and are varied from labradorite to andesine. They occur as phenocrysts (1-5mm), microphenocrsyts (0.04 to 0.07 mm long and 0.01-0.02 mm wide) and microlites in groundmass. Although plagioclases show sign of resorption, microphenocryst grains are mostly the resorbed ones. Plagioclases are either elongated lath shape or euhedral to subhedral tabular-shaped grains. The interior of plagioclases is usually clear or contain enclaves of pyroxene and glass. Many phenocrysts have overgrowths and dusty cores or outer margins (sieve texture) similar to plagioclase morphology in andesites reported in other studies [32, 50, 58 and 48]. The dust materials are mainly glass, alkali feldspar, quartz and other fine-grained minerals [36]. Sieve-textured core and sieve-ringed plagioclase are indicating partial resorption which varies in thickness.

The plagioclases in the host rock and enclaves are quite similar and can be divided into three categories based on their textures (Fig. 5): Type 1 plagioclase with a clear core ($An_{53.94-88.87}$) bounded by a dusty/cellular zone (resorption rim) ($An_{43.81-62.30}$) that in turn is bounded by a clear overgrowth rim ($An_{46.92-71.00}$) (Fig. 5a). Type 2 plagioclase is characterized by dusty/cellular core ($An_{50.23-63.89}$) bounded by a clear overgrowth rim ($An_{45.96-57.91}$) that in turn bounded by dusty rim ($An_{47.71-62.46}$) (Fig. 5b). In type 2 plagioclase the sieved texture also results from the presence of abundant glass (melt) that permeates the crystal interior (Fig. 5c). In both type 1 and 2 plagioclase multiple layers of dusty and clear zones, which are signs of complex reaction and crystallization are obvious [50]. Type 3 is the most common population of plagioclase and is characterized by the overall absence of dusty or cellular textures and overgrowth ($Anc_{44.87-91.05}$, $Ane_{49.62-67.36}$) (Fig. 5d). Grain interiors are comparatively clean and uniform but can be zoned or twinned. The oacillatory zoning is common and the grains occasionally form glomeroporphyritic aggregates by themselves or with pyroxene grains. Plagioclase microphenocryts have similar composition with larger phenocrysts. Groundmass plagioclase microlites have a compositional range of $An_{45.86-54.91}$. Fine lath plagioclase microlites in the graoundmass are often deviate around various kinds of phenocrysts, producing a pilotaxitic texture.

Pyroxenes

Pyroxenes account for 15-20 vol% of rock samples. Clinopyroxenes are generally more abundant than orthopyroxenes and both are found in glomeroporphyritic aggregates with plagioclase and Fe-Ti oxides. They occur as fine grains <0.1 mm in the groundmass and as prismatic to rectangular subhedral to euhedral phenocrysts, 1 to 3 mm, and sometimes slightly larger in clusters. Some grains are partly resorbed and commonly contain enclaves of plagioclase and Fe-Ti oxide. The pyroxene compositions (Tables 2 and 3) are shown in Fig. 4b. Both orthopyroxene, ranging in composition $En_{59.67}$ to $En_{73.30}$ (classified mainly as hyperstine with few grading toward bronzite, following Morimoto et al., [44]) as well as clinopyroxene $Wo_{40.88-46.00}$, $Fs_{11.08-17.07}$, $En_{36.69-47.85}$ (classified mainly as augite with few grading toward salite, following Morimoto et al., [44]) are dominated by quadrilateral components and are similar to pyroxenes of typical orogeneic andesites [28,46,50].

The optical compositional zoning is rare in majority of pyroxene crystals but some grains exhibit reverse zoning with iron-rich cores and more magnesium rims

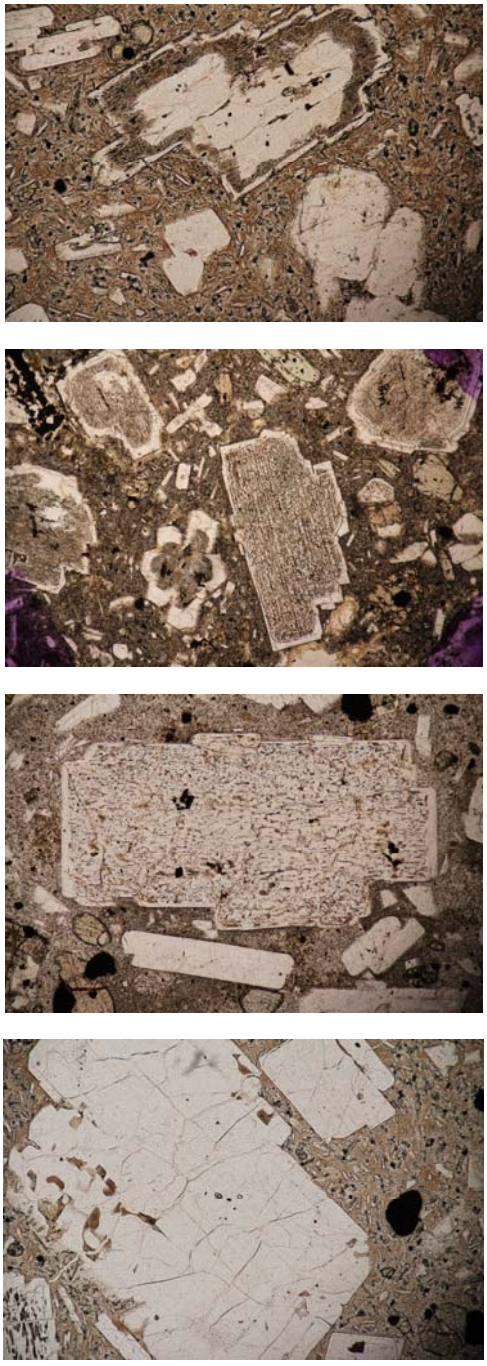

Figure 5. Photomicrogrphs (in plane-polarized light with field of view is 10 mm across) of the three populations (see text) of plagioclase phenocrysts: (a) Showing the fresh core of plagioclase grains surrounded by the dusty zone which in turn fringed by a thin clear rim. (b) Showing that the dusty zone occurs at the center of the grains whereas the fresh plagioclase occurs towards the border of the plagioclase grains. (c) Showing sieve-cored, where the sieved texture resulted from presence of abundant glass (melt) that permeates the crystal interior. (d) Unsieved, with no dissolution texture.

Table 2. Representative electron microprobe (oxides in wt%) analyses of clinopyroxene from Rabor andesites

Sample	S-11-1								S-11-2		
Grain	C1	C2		C3			C4		C5	C6	C7
Position	(Enclave)	(Enclave)		(Host)			(Host)		(Enclave)	(Enclave)	(Host)
	In plagioclase	Edge (Dark)	Core (Bright)	Edge (Dark)	Middle (Bright)	Core (Bright)	Edge	Core			
SiO_2	51.75	51.87	50.37	52.6	51.36	52.88	52.79	53.2	52.34	52.37	52.45
TiO_2	0.544	0.5045	0.8361	0.3855	0.4449	0.2864	0.2296	0.2615	0.3626	0.3447	0.4593
Al_2O_3	1.6174	2.0391	3.36	2.1039	1.9887	1.1829	0.7759	0.8327	1.2176	1.3469	1.3802
Cr_2O_3	0	0	0.1256	0.1552	0.0329	0.0376	0.0179	0	0.018	0.0165	0
FeO	10.02	9.56	9.79	7.41	8.63	8	10.07	8.86	8.89	8.09	9.4
MgO	13.45	14.07	12.78	16.44	14.08	14.98	14.05	14.35	14.06	14.5	14.13
MnO	0.2918	0.2871	0.2336	0.1627	0.2485	0.2697	0.3334	0.2112	0.2624	0.1888	0.2635
NiO	0	0	0.0309	0	0	0	0.0269	0.0469	0	0	0
CaO	20.38	21.19	21.27	19.91	21.01	21.31	20.94	21.28	21.49	20.58	20.81
Na_2O	0.3269	0.3044	0.3722	0.1678	0.3658	0.281	0.2784	0.2926	0.2783	0.251	0.2969
Total	98.38	99.82	99.16	99.34	98.16	99.23	99.51	99.33	98.93	97.69	99.18
Si	1.9649	1.9414	1.9046	1.9479	1.9475	1.9747	1.9836	1.9905	1.9712	1.9825	1.9699
Ti	0.0155	0.0142	0.0238	0.0107	0.0127	0.008	0.0065	0.0074	0.0103	0.0098	0.013
Al	0.0724	0.0899	0.1497	0.0918	0.0889	0.0521	0.0344	0.0367	0.054	0.0601	0.0611
Cr	0	0	0.0038	0.0045	0.001	0.0011	0.0005	0	0.0005	0.0005	0
Fe	0.3182	0.2992	0.3095	0.2295	0.2738	0.2498	0.3163	0.2771	0.2801	0.2561	0.2953
Mg	0.7615	0.7847	0.72	0.9076	0.7961	0.8337	0.7868	0.8002	0.7893	0.8185	0.7909
Mn	0.0094	0.0091	0.0075	0.0051	0.008	0.0085	0.0106	0.0067	0.0084	0.0061	0.0084
Ni	0	0	0.0009	0	0	0	0.0008	0.0014	0	0	0
Ca	0.8293	0.8499	0.8615	0.7899	0.8536	0.8527	0.8429	0.8531	0.8672	0.8346	0.8373
Na	0.0241	0.0221	0.0273	0.012	0.0269	0.0203	0.0203	0.0212	0.0203	0.0184	0.0216
O	6	6	6	6	6	6	6	6	6	6	6
CatTot	3.995	4.01	4.009	3.999	4.008	4.001	4.003	3.994	4.001	3.987	3.997
Total	9.995	10.01	10.009	9.999	10.008	10.001	10.003	9.994	10.001	9.987	9.997
Mg	39.69454	40.38808	37.92468	46.97479	41.21667	42.87037	40.21261	41.30917	40.58098	42.73482	40.93897
Fe	17.07673	15.86803	16.69739	12.14223	14.5897	13.28225	16.70755	14.65077	14.8329	13.68976	15.72028
Ca	43.22873	43.74389	45.37793	40.88298	44.19363	43.84738	43.07983	44.04006	44.58612	43.57542	43.34075

(Table 2), which is also apparent in back-scattered electron (BSE) images (Fig. 6). The cores are compositionally uniform and the magnesian rims are normally slightly zoned. Generally pyroxenes show very uniform chemical composition, although, symplectitic intergrowths of pyroxene (host) with magnetite and/or ilmenite (vermicules) have been observed. This has been considered to result from the subsolidus oxidation of titanomagnetite included in the orthopyroxene [33], or to be resulted from a simultaneous magmatic crystallization, that of the oxide minerals being crystallized faster [20].

Glass

Glasses occur both in the groundmass and as inclusions in plagioclase. In major element terms, the glass in Rabor pyroxene andesites are mainly high-Si rhyolites (76.31-81.67 wt% SiO_2) while in enclaves they

Table 2. Continue

Sample	S-11						S25					
Grain	C8	C9	C10	C11			C12	C13	C14	C15	C16	C17
Position	(Enclave)	(Host)	(Enclave)	(Host)			(Enclave)	(Enclave)	(Enclave)	(Host)	(Enclave)	(Host)
				Edge	Middle	Core					In plagioclase	
SiO_2	51.84	52.74	52.93	51.98	49.49	47.5	52.59	52.51	52.42	52.67	52.42	51.83
TiO_2	0.5789	0.3688	0.3739	0.4104	0.9228	1.5371	0.1762	0.3674	0.4104	0.3126	0.2953	0.5216
Al_2O_3	2.3847	1.2433	1.1574	2.7668	4.93	6.74	0.7591	1.137	1.5599	1.039	1.4748	1.9684
Cr_2O_3	0.1053	0.0195	0	0.1129	0.084	0.039	0.0285	0.0404	0.0135	0.015	0.0045	0.021
FeO	8.85	9.47	8.98	6.62	7.4	8.2	9.31	9.4	8.23	8.73	8.74	8.34
MgO	13.95	14.25	14.3	16.38	14.39	12.84	14.82	14.19	14.52	14.52	14.56	14.17
MnO	0.1879	0.3077	0.3115	0.1432	0.1059	0.199	0.3125	0.2408	0.2234	0.202	0.2653	0.2255
NiO	0	0	0.0539	0.013	0.0129	0.0299	0.023	0.0389	0.011	0.004	0.002	0
CaO	21.33	20.64	20.85	19.55	20.6	20.49	20.93	20.44	20.83	21.13	23.25	20.81
Na_2O	0.3451	0.3069	0.2688	0.2203	0.2714	0.2786	0.2853	0.2787	0.2835	0.24	0.2651	0.295
Total	99.57	99.36	99.22	98.19	98.20	97.85	99.23	98.65	98.50	98.85	101.28	98.19
Si	1.9389	1.9766	1.9825	1.9391	1.8647	1.8074	1.9761	1.9809	1.9712	1.9795	1.9379	1.9581
Ti	0.0163	0.0104	0.0105	0.0115	0.0261	0.044	0.005	0.0104	0.0116	0.0088	0.0082	0.0148
Al	0.1051	0.0549	0.0511	0.1216	0.2187	0.3021	0.0336	0.0505	0.0691	0.046	0.0643	0.0876
Cr	0.0031	0.0006	0	0.0033	0.0025	0.0012	0.0008	0.0012	0.0004	0.0004	0.0001	0.0006
Fe	0.2767	0.2968	0.2812	0.2065	0.2333	0.2609	0.2924	0.2966	0.2589	0.2743	0.2701	0.2635
Mg	0.7777	0.7962	0.7983	0.9106	0.808	0.7285	0.83	0.7979	0.8141	0.8132	0.8023	0.7979
Mn	0.006	0.0098	0.0099	0.0045	0.0034	0.0064	0.0099	0.0077	0.0071	0.0064	0.0083	0.0072
Ni	0	0	0.0016	0.0004	0.0004	0.0009	0.0007	0.0012	0.0003	0.0001	0.0001	0
Ca	0.8545	0.8289	0.8365	0.7814	0.8315	0.8352	0.8427	0.8262	0.8392	0.8507	0.9209	0.8424
Na	0.025	0.0223	0.0195	0.0159	0.0198	0.0206	0.0208	0.0204	0.0207	0.0175	0.019	0.0216
O	6	6	6	6	6	6	6	6	6	6	6	6
CatTot	4.003	3.996	3.991	3.995	4.008	4.007	4.012	3.993	3.993	3.997	4.031	3.994
Total	10.003	9.996	9.991	9.995	10.008	10.007	10.012	9.993	9.993	9.997	10.031	9.994
Mg	40.61309	41.21758	41.45075	47.85076	43.06577	39.787	42.02532	41.37627	42.41651	41.81837	40.08293	41.75301
Fe	14.76317	15.87203	15.11501	11.08776	12.61593	14.59858	15.30633	15.77992	13.85922	14.43485	13.90887	14.16536
Ca	44.62374	42.91039	43.43424	41.06148	44.3183	45.61442	42.66835	42.84381	43.72427	43.74679	46.00819	44.08163

are less silicic (~5.00 wt%) than groundmass glasses in host andesite (Table 4).

Result and Discussion

Evidence of Magma Mixing and Mingling

The term ‘magma mingling’ as used here refers to the formation of discrete inclusions by quenching of hotter magma in a lower temperature magma [7]. The process of complete mixing of two magmas to form a new magma is termed ‘hybridization’, which commonly comprising crystals from the two end-member magmas.

The Miocene Rabor pyroxene andesite lava flows contain numerous dark grey color igneous enclaves in places in the upper section. The bulk rock compositions of the Rabor pyroxene andesite and its igneous enclaves are almost indistinguishable from one another (though the enclaves have slightly higher SiO_2 and K_2O content) and both plot in the field of andesite in total alkali-silica (TAS) diagram of Le Maitre [41]. In general the Rabor pyroxene andesites are more silicic (SiO_2% = 56.1-61.9) and all are medium-k calc-alkaline according to Gill [28]. They have trace element characteristics of typical

Table 3. Representative electron microprobe (oxide in wt%) analyses of orthopyroxene from Rabor andesites

Sample	S-11-1											S-11-2		
Grain	O1	O2	O3	O4	O5	O6	O7	O8	O9	O10	O11	O12	O13	
Position	(Enclave)	(Enclave)	(Enclave)	(Enclave)	(Enclave)	(Enclave)	(Host)	(Host)	(Host) In plagioclase	(Host)	(Host)	(Enclave)	(Enclave) Edge	(Enclave) Core
SiO_2	52.63	52.79	53.77	53.22	53.41	53.53	53.32	53.09	52.79	53.16	52.92	52.28	53.76	52.47
TiO_2	0.2922	0.2795	0.1666	0.2637	0.2739	0.2431	0.2164	0.2561	0.2166	0.2776	0.2543	0.3295	0.1776	0.3078
Al_2O_3	0.9176	0.7668	0.6875	1.0191	1.0036	0.6554	0.6652	0.9593	1.0481	0.7927	0.7228	1.1613	0.6921	1.1275
Cr_2O_3	0	0	0.0313	0.027	0.0085	0	0.0042	0.0156	0.0014	0	0	0.031	0	0.0028
FeO	21.59	22.16	21.16	21.35	21.27	22.38	22.74	22.53	22.13	21.51	23.27	23.02	21.12	22.64
MgO	22.33	21.85	23.06	22.26	22.68	22.53	22.03	21.91	21.78	22.88	22.09	21.13	22.83	20.84
MnO	0.5847	0.6768	0.6079	0.67	0.6836	0.6337	0.616	0.6848	0.6503	0.6408	0.729	0.4851	0.6788	0.5759
NiO	0.027	0.013	0	0	0.036	0	0	0.018	0.0509	0	0.0358	0	0.003	0.014
CaO	1.5007	1.5549	1.1963	1.5246	1.437	1.43	1.3778	1.5711	1.3035	1.255	1.3223	1.9011	1.1491	1.7794
Na_2O	0.009	0	0.0006	0.0163	0.0123	0.0115	0.0154	0.0054	0.0225	0.0463	0.0176	0.0297	0.0239	0.0399
Total	99.88	100.10	100.68	100.34	100.81	101.41	100.98	101.04	99.99	100.56	101.36	100.37	100.43	99.80
Si	1.964	1.9709	1.9804	1.972	1.9689	1.9709	1.9746	1.9656	1.9704	1.9669	1.9605	1.956	1.9847	1.9696
Ti	0.0082	0.0078	0.0046	0.0074	0.0076	0.0067	0.006	0.0071	0.0061	0.0077	0.0071	0.0093	0.0049	0.0087
Al	0.0404	0.0337	0.0298	0.0445	0.0436	0.0284	0.029	0.0419	0.0461	0.0346	0.0316	0.0512	0.0301	0.0499
Cr	0	0	0.0009	0.0008	0.0002	0	0.0001	0.0005	0	0	0	0.0009	0	0.0001
Fe	0.6737	0.692	0.6517	0.6616	0.6556	0.6892	0.7044	0.6976	0.6908	0.6657	0.7208	0.7202	0.652	0.7107
Mg	1.2418	1.216	1.266	1.2295	1.2461	1.2362	1.2161	1.2089	1.2119	1.2617	1.2196	1.1784	1.2559	1.166
Mn	0.0185	0.0214	0.019	0.021	0.0213	0.0198	0.0193	0.0215	0.0206	0.0201	0.0229	0.0154	0.0212	0.0183
Ni	0.0008	0.0004	0	0	0.0011	0	0	0.0005	0.0015	0	0.0011	0	0.0001	0.0004
Ca	0.06	0.0622	0.0472	0.0605	0.0568	0.0564	0.0547	0.0623	0.0521	0.0498	0.0525	0.0762	0.0454	0.0716
Na	0.0007	0	0	0.0012	0.0009	0.0008	0.0011	0.0004	0.0016	0.0033	0.0013	0.0022	0.0017	0.0029
O	6	6	6	6	6	6	6	6	6	6	6	6	6	6
CatTot	4.008	4.004	4	3.999	4.002	4.009	4.005	4.006	4.001	4.01	4.017	4.01	3.996	3.998
Total	10.008	10.004	10	9.999	10.002	10.009	10.005	10.006	10.001	10.01	10.017	10.01	9.996	9.998
Mg	62.86004	61.71962	64.43076	62.99959	63.62522	62.37764	61.56845	61.40289	61.99611	63.81246	61.19725	59.67187	64.29632	59.84705
Fe	34.10276	35.12334	33.16708	33.90039	33.4746	34.77647	35.66221	35.43275	35.33865	33.66882	36.1684	36.46952	33.37941	36.47796
Ca	3.037206	3.15704	2.402158	3.10002	2.900179	2.845898	2.76934	3.164364	2.665234	2.518713	2.634352	3.858619	2.324272	3.674999

subduction related volcanic rocks (high LILE/HFSE ratios, enrichment of LILE) (Dargahi and Arvin in preparation).The enclaves are not homogeneously distributed in the lava flow. They form thin ribbons, spherical to ellipsoid and some angular shapes. They have sharply defined smooth contacts with the host andesite magma and some show well-defined chilled margins. Where two types of enclaves are seen together, the merging of spherical to ellipsoidal enclaves leads to the formation of ribbon enclave and their detachment from ribbon enclave leads to its disintegration. Mineralogically, the host andesite is composed of plagioclase, clinopyroxene, orthopyroxene and magnetite that form phenocrysts and microphenocrysts set in a glassy microlitc groundmass of the same minerals. The enclaves are more crystallized, have the same mineralogy as the host andesite with less glassy matrix. Compositionally, the mineral phases in the host andesite and the enclaves are overlapping each other.

Plagioclases show a relatively large range of anorthite content (An_{43-91}) and varied mostly from andesine to labradorite in composition. They show a clear evidence of multiple origin and periods of dissolution and growth. Fine grained resorption zones in

Table 3. Continue

Sample	S-11-2				S-11			S-14						S-25
Grain	O14	O15	O16	O17	O18	O19	O20	O21	O22	O23	O24	O25	O26	O27
Position	(Host)	(Enclave)	(Enclave)	(Host)	(Host)	(Enclave)	(Host)	(Enclave)	(Enclave)	(Host)	(Enclave)	(Host)	(Host)	(Enclave)
SiO_2	53.02	53.06	52.84	53.6	53.17	53.26	53.57	54.02	52.72	54.11	53.72	54.06	53.16	52.82
TiO_2	0.3083	0.2708	0.2917	0.2689	0.2865	0.2212	0.2652	0.1789	0.2021	0.2209	0.281	0.2383	0.2173	0.2452
Al_2O_3	0.9768	0.9382	0.7712	0.9073	0.7911	1.2175	0.9642	0.6031	0.6439	1.0103	0.9764	0.9672	0.8092	0.8285
Cr_2O_3	0	0	0.0196	0	0.0184	0	0	0	0	0.0172	0.0214	0	0.0127	0.0142
FeO	21.56	22.37	23.78	21.15	21.94	21.02	19.85	20.71	20.63	19.27	19.48	18.72	22.3	20.29
MgO	23.02	21.89	21.84	23.52	22.51	23.82	23.75	23.2	22.2	24.8	23.44	24.38	21.4	23.04
MnO	0.447	0.5918	0.6737	0.6095	0.4931	0.6258	0.5591	0.5175	0.6168	0.5447	0.5579	0.4968	0.615	0.5596
NiO	0.015	0	0.0109	0.011	0	0.0309	0	0.0219	0.0169	0	0.0359	0.0189	0.0169	0.008
CaO	1.4868	1.583	1.4404	1.2705	1.6637	0.9141	1.3714	1.2672	1.3198	1.2882	1.2731	1.1906	1.2575	1.2544
Na_2O	0.0742	0	0	0.0195	0.0234	0.0469	0.007	0.0081	0.0103	0.0216	0.105	0.023	0.0248	0.0407
Total	100.91	100.70	101.66	101.36	100.9	101.17	100.34	100.53	98.36	101.28	99.89	100.10	99.82	99.10
Si	1.9561	1.9686	1.9562	1.9627	1.9654	1.9524	1.9695	1.9872	1.987	1.9641	1.9798	1.9788	1.9868	1.9725
Ti	0.0086	0.0076	0.0081	0.0074	0.008	0.0061	0.0073	0.005	0.0057	0.006	0.0078	0.0066	0.0061	0.0069
Al	0.0425	0.041	0.0337	0.0392	0.0345	0.0526	0.0418	0.0262	0.0286	0.0432	0.0424	0.0417	0.0356	0.0365
Cr	0	0	0.0006	0	0.0005	0	0	0	0	0.0005	0.0006	0	0.0004	0.0004
Fe	0.6654	0.694	0.7362	0.6478	0.6783	0.6445	0.6104	0.6373	0.6503	0.5849	0.6004	0.5732	0.6969	0.6339
Mg	1.2657	1.2105	1.2052	1.2835	1.2403	1.3016	1.3016	1.2721	1.2474	1.3417	1.2874	1.3301	1.192	1.2825
Mn	0.014	0.0186	0.0211	0.0189	0.0154	0.0194	0.0174	0.0161	0.0197	0.0167	0.0174	0.0154	0.0195	0.0177
Ni	0.0004	0	0.0003	0.0003	0	0.0009	0	0.0006	0.0005	0	0.0011	0.0006	0.0005	0.0002
Ca	0.0588	0.0629	0.0571	0.0498	0.0659	0.0359	0.054	0.0499	0.0533	0.0501	0.0503	0.0467	0.0504	0.0502
Na	0.0053	0	0	0.0014	0.0017	0.0033	0.0005	0.0006	0.0008	0.0015	0.0075	0.0016	0.0018	0.0029
O	6	6	6	6	6	6	6	6	6	6	6	6	6	6
CatTot	4.017	4.003	4.019	4.011	4.01	4.017	4.003	3.995	3.993	4.009	3.995	3.995	3.99	4.004
Total	10.017	10.003	10.019	10.011	10.01	10.017	10.003	9.995	9.993	10.009	9.995	9.995	9.99	10.004
Mg	63.60621	61.5279	60.30523	64.78724	62.49937	65.67104	66.20549	64.92625	63.93644	67.87575	66.42588	68.21026	61.46548	65.21408
Fe	33.43887	35.27498	36.83763	32.69901	34.17989	32.51766	31.04781	32.52692	33.33162	29.58972	30.97879	29.39487	35.93565	32.2333
Ca	2.954922	3.197113	2.857143	2.513755	3.320736	1.811302	2.746694	2.546828	2.731932	2.534527	2.595325	2.394872	2.598876	2.552629

plagioclase are probably caused by superheating, as suggested by Tsuchiyama [68]. Oscillatory zoning in plagioclase phenocrysts is likewise ambiguous to interpret as it can result from temperature or PH_2O fluctuations that could arise from thermal convection [67, 32, 19, 29], heating due to decompression induced crystallization [13] or pressure changes induced by eruption [34 and 60]. However, the lack of enrichment of magmatic PH_2O in the Rabor pyroxene andesites may explain the absence of hornblende and olivine, existing of few pyroxene phenocrysts with Mg-rich rims, low amount of magnetite crystallization, and non-occurrence of orthopyroxene phenocrysts rimmed with clinopyroxne. Pyroxenes generally show a uniform chemical composition and classified mainly as hypersthene ($En_{59.67}$ to $En_{73.30}$) and augite ($Wo_{40.88\text{-}46.00}$, $Fs_{11.08\text{-}17.07}$, $En_{36.69\text{-}47.85}$). Some pyroxene phenocrysts exhibit reverse zoning with iron rich cores and more magnesia rims. The formation of reversely zoned pyroxene phenocrysts like the ones in the Rabor pyroxene andesitic rocks can be explained by changing oxidation estates during crystallization [32, 60], suggesting more oxidizing conditions. Therefore, petrographic features as well as composition of phenocrysts clearly exhibit disequilibrium conditions in the Rabor pyroxene andesite.

Table 3. Continue

Sample	S-25								
Grain	O28		O29	O30	O31	O32	O33	O34	O35
Position	(Enclave)		(Enclave)	(Enclave)	(Enclave)	(Enclave)	(Host)	(Enclave)	(Host)
	Core	Edge							
SiO_2	52.63	53.89	53.66	53.75	53.37	52.59	53.46	52.69	54.14
TiO_2	0.3118	0.2011	0.2454	0.2247	0.2941	0.3471	0.2016	0.1784	0.1834
Al_2O_3	2.4475	1.2643	0.7453	0.7271	0.7286	0.8573	0.6148	0.7426	0.5611
Cr_2O_3	0.0029	0.0359	0	0	0	0	0	0.0099	0.0057
FeO	15.37	15.95	20.49	19.83	20.45	21.16	19.1	19.82	17.95
MgO	26.24	26.16	22.93	22.78	22.81	21.28	22.41	21.53	24.17
MnO	0.424	0.3759	0.5073	0.5254	0.5374	0.5469	0.4864	0.51	0.5599
NiO	0.0389	0.0288	0.0555	0.0209	0	0	0	0	0.0159
CaO	0.7008	0.8052	1.3492	1.3399	1.417	1.4309	1.2361	1.4984	1.2495
Na_2O	0.025	0.0907	0.088	0.0469	0.0087	0.0534	0.0398	0.0184	0.0157
Total	98.20	98.79	100.07	99.25	99.62	98.27	97.55	97.00	98.85
Si	1.935	1.9718	1.9835	1.9957	1.9821	1.9885	2.0116	2.0048	1.9997
Ti	0.0086	0.0055	0.0068	0.0063	0.0082	0.0099	0.0057	0.0051	0.0051
Al	0.1061	0.0545	0.0325	0.0318	0.0319	0.0382	0.0273	0.0333	0.0244
Cr	0.0001	0.001	0	0	0	0	0	0.0003	0.0002
Fe	0.4727	0.488	0.6333	0.6157	0.635	0.6691	0.601	0.6306	0.5545
Mg	1.4381	1.4267	1.2631	1.2604	1.2629	1.1995	1.2567	1.221	1.331
Mn	0.0132	0.0117	0.0159	0.0165	0.0169	0.0175	0.0155	0.0164	0.0175
Ni	0.0011	0.0008	0.0017	0.0006	0	0	0	0	0.0005
Ca	0.0276	0.0316	0.0534	0.0533	0.0564	0.058	0.0498	0.0611	0.0495
Na	0.0018	0.0064	0.0063	0.0034	0.0006	0.0039	0.0029	0.0014	0.0011
O	6	6	6	6	6	6	6	6	6
CatTot	4.004	3.998	3.997	3.984	3.994	3.985	3.971	3.974	3.983
Total	10.004	9.998	9.997	9.984	9.994	9.985	9.971	9.974	9.983
Mg	74.19005	73.30319	64.781	65.32601	64.6216	62.25994	65.88204	63.83646	68.78553
Fe	24.38609	25.07322	32.48025	31.91148	32.49245	34.72958	31.50721	32.9691	28.65633
Ca	1.423855	1.623593	2.738742	2.762517	2.885944	3.010485	2.610747	3.194437	2.55814

Reverse zoning in pyroxene and oscillatory zoned and dusty sieve-textured plagioclase, similar to Rabor pyroxene andesite, have been reported from many mingled and hybrid magmas [37, 46, 6, 51] where magma mixing has been proposed as the dominant cause for the development of such observed phenomena [32, 52, 30, 34, 49, 50, 66, 48]. Therefore, with the careful field observation and detailed laboratory analyses, it is safe to speculate that Rabor pyroxene andsite represents a mixing or mingling between mafic and silicic magmas with different temperatures and compositions, as has been suggested for the origin of similar andesites from various localitions around the world [32, 6, 47, 52, 38] . The fact that rhyolite glass is also present in the Rabor pyroxene andesite also supports this conclusion.

The enclaves with coherent and sharp contact with the host andesite, the remarkably spherical and ribbon shape enclaves with abnormally darker color compared to the host rock, the lack of a rapid crystallization texture (e.g., matted pyroxene and acicular plagioclase with interstitial glass) and the fact that the mineral phases in the host andesite and the enclaves overlap, confirm that the enclaves and the host andesite are cogenetic.

Table 4. Representative electron microprobe (oxides in wt%) analyses of glass from Rabor andesites

Sample	S-11-1			S-11-2			S-11		S-25		
Grain	G1	G2	G3	G4	G5	G6	G7	G8	G9	G10	G11
Position	(Enclave) In plagioclase	(Enclave)	(Host)	(Host)	(Host)	(Host)	(Host)	(Host)	(Enclave)	(Host)	(Enclave)
SiO_2	76.31	77.50	81.67	80.37	80.17	80.07	80.25	81.05	76.86	81.03	77.61
TiO_2	0.4959	0.5067	0.4433	0.4844	0.5023	0.4851	0.4865	0.4914	0.4499	0.4142	0.0594
Al_2O_3	12.94	12.68	10.58	10.55	11.7	10.53	11.78	11.73	12.96	10.78	12.43
FeO	1.3144	0.9908	0.7417	0.6143	0.6548	0.7074	0.8384	0.6746	1.239	1.2663	0.0071
MgO	0.0907	0.0588	0.0197	0.0166	0.0207	0.0257	0.0504	0.0113	0.1046	0.1248	0.0703
MnO	0.0353	0.0012	0.0020	0.0060	0.0402	0.0206	0.0267	0.0146	0.0061	0.0654	0.0098
CaO	0.415	0.2968	0.2741	0.2753	0.4161	0.2706	0.3103	0.2986	0.3711	0.0142	0.5038
Na_2O	2.7123	2.7993	2.3536	2.9515	2.3076	2.3849	2.6247	2.0178	2.2582	2.5511	2.604
K_2O	3.989	3.3689	2.5801	3.2126	2.8816	2.5865	3.1479	3.159	3.3273	3.2314	4.4
Total	98.30	98.20	98.66	98.48	98.69	97.08	99.51	99.44	97.57	99.47	97.69

Evolution of Enclaves

The presence of mafic magmatic inclusions, or enclaves, has been recognized as evidence of mixing between two at least partially molten magmas [e.g., 23, 24, 8, 7, 64, 17, 46, 18]. From the various textures of enclaves, it seems we are looking at a magmatic emulsion with suspended droplet ofone magma in another. The fact that there is a limited amount of mixing reflects a viscosity contrast due to higher liquidus temperature of intruded magma relative to the host andesitic magma. Therefore, we propose the following model for the formation of these abnormal andesitic enclaves in the Rabor pyroxene andesite host. Before reheating, the host andesitic magma was partially molten and in a crystallization status. The rounded enclaves are likely to represent quenched blobs of intruding new andesite magma with higher liquidus that have been incorporated into the host andesitic magma in a liquid or near liquid state, as evidenced by the enclave sizes and by the presence of chilled margins on some enclaves.

The blobs are unusually small, which reflect a small viscosity contrast and some turbulence during mixing. The small size and rounded shape of enclaves imply a non-Newtonian behavior within the host andesite magma [59, 11, 12]. Their temperature differences with the host magma permits buoyant uprising of enclaves [46]. Intrusion of fresh magma could also result in convection in the andesitic host magma chamber. There is evidence of "crystal capture", some of the blobs have entrained the crystals which were originally present in the host magma at the time of mingling while others have escaped from them and got into the host magma. Circling microlites inside the enclaves are further evidence for convection in the andesitic host magma. (Fig. 3a), Petrographic study shows that the ribbon type enclaves have been formed by merging of rounded blobs.

a)

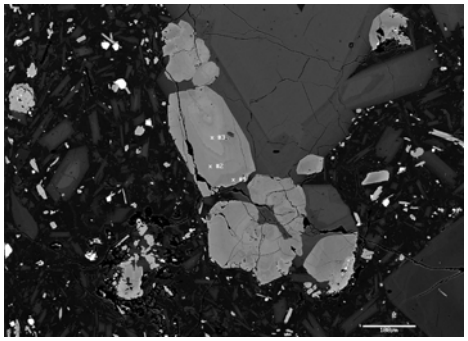

b)

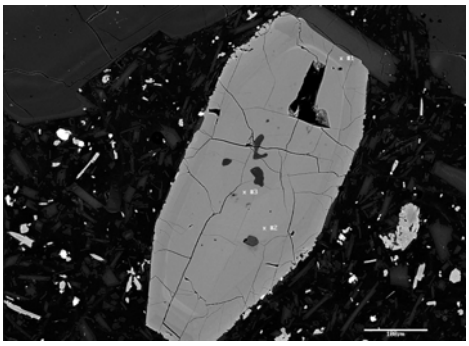

Figure 6. Back-scattered electron images of pyroxenes. (a) Reverse zoning in hypersthene. The magnesian rim surrounds the Fe-rich core. (b) Reverse zoning in augite where the texture resembles that of hypersthene.

Crystallization of the enclave groundmass is possible by the temperature contrast between the replenishing and host magmas [7]. Groundmass textures and crystal morphologies observed in the enclaves indicate the degree of undercooling between the enclaves and the host [7 and 43]. The more crystalline and microlitic nature of the enclaves can be explained by (a), the similarity of the host and enclave melts which suggests that thermal equilibrium between the two has been reached and enclave groundmass has been crystallized to a greater extent than the host groundmass [18] and (b), the growth of microlites in the magma is thought to have occurred either during ascent of magmas to the surface, or during storage in a shallow, subsurface chamber [16,27,18].

In summary, the available geological, petrography and electron microprobe data of Rabor pyroxene andesitic rocks lead to the conclusions that:

- textural relationship and composition of mineral phases suggest the existence of disequilibrium crystallization and a complex history of magma mixing and mingling;
- the enclaves and andesite host rocks are cogentic;
- enclaves show evidence of melting during incorporation into andesite and are believed to represent quenched blobs of andesite magma with higher liquidus temperature that was integrated into the host andesitic magma in a liquid or near liquid state;
- similarity of host and enclave melts and the growth of the microlites in enclave magma, either during ascent or storage in a shallow subsurface chamber, explain the more crystalline nature of the enclaves and their microlitic groundmass.

Acknowledgements

We gratefully acknowledge the Vice Chancellor of Research and Technology at Shahid Bahonar University of Kerman and the Natural Science and Engineering Research Council (NSERC) of Canada for their financial supports. The authors are thankful to Tom Bonli for electron microprobe analysis and Blaine Novakovski for preparation of the thin-polished sections at the University of Saskatchewan.

References

1. Agard, P., Omrani, J., Jolivet, L. and Mouthereau, F. Convergence history across Zagros (Iran): constraints from collisional and earlier deformation. International Journal of Earth Sciences, **94:** 401-419 (2005).
2. Agard, P., Omrani, J., Jolivet, L., Whitechurch, H., Vrielynck, B., Spakman, W., Monie, P., Meyer, B. and Wortel, R. Zagros orogeny: a subduction-dominated process. Geological Magazine, **148:** 692-725 (2011).
3. Ahmad, T. and Posht Kuhi, M. Geochemistry and petrogenesis of the Urumiah- Dokhtar volcanic belt around Nain and Rafsanjan area; a preliminary study: Treatise on the geology of Iran. Iranian Ministry of Mines and Metals 90 p. (1993).
4. Alavi, M. Tectonics of the Zagros orogenic belt of Iran: new data and interpretations. Tectonophysics, **229:** 211–238 (1994).
5. Alavi, M. Regional stratigraphy of the Zagros fold-thrust belt of Iran and its proforeland evolution. American Journal of Science, **304:** 1-20 (2004).
6. Alpaslan, M., Ekici, T., Otlu, N., Boztug, D. and Temel, A. Magmatic processes and mixing origin of ansedite: Miocene Karamagara volcanics, Central Anatolia, Turkey. Geological Journal, **40:** 193-214 (2005).
7. Bacon, C. R. Magmatic inclusions in silicic and intermediate volcanic rocks. Journal of Geophysical Research, **91:** 6091-6112 (1986).
8. Bacon, C. R. and Metz, J. Magmatic inclusions in rhyolites, contaminated basalts, and compositional zonation beneath the Caso Volcanic Field California. Contributions to Mineralogy and Petrology, **85:** 346-365 (1984).
9. Berberian, M. and King, G. C. P. Towards a paleogeography and tectonic evolution of Iran. Canadian Journal of Earth Sciences, **18:** 210-265 (1981).
10. Berbberian, F., Muir, I. D., Pankhurst, R. J. and Berbberian, M. Late Cretaceous and early Miocene Andian type plutonic activitiy in northern Makran and central Iran. Journal of Geological Society of London, **139:** 605-614 (1982).
11. Bindeman, I. N. and Baily, J. C. A model of reverse differentiation at Dikkii Greben volano, Kamchatka: progressive basic magma vesiculation in a silicic magma chamber. Contributions to Mineralogy and Petrology, **117:** 263-278 (1994).
12. Blake, S. and Fink, H. H. On the deformation and freezing of enclaves during magma mixing. Journal of Volcanology and Geothermal Research, **95:** 1-8 (2000).
13. Blundy, J., Cashman, K. and Humphreys, M. Magma heating by decompression-driven crystallisation beneath andesite volcanoes. Nature, **443:** 76-80 (2006).
14. Browne, B. L., Eichelberger, J. C., Patino, L. C., Vogel, T. A., Dehn, J., Uto, K. and Hoshizuni, H. Generation of porphyritic and equigranular mafic enclaves during magma recharge events at Unzen Volcano, Japan. Journal of Petrology, **47:** 301-328 (2006).
15. Browne, B. L., Eichelberger, J. C., Patino, L. C., Vogel, T. A., Uto, K. and Hoshizuni, H. Magma mingling as indicated by texture and Sr/Ba ratios of plagioclase phenocrysts from Unzen Volcano, SW Japan. Journal of Volcanology and Geothermal Research, **154:** 103-116 (2006).
16. Cashman, K. V. Groundmass crystallization of Mount St. Helen dacite, 1980-1986: A tool for interpreting shallow magmatic processes. Contributions to Mineralogy and Petrology, **109:** 431-449 (1992).
17. Clynne, M. A complex magma mixing origin for rocks

erupted in 1915, Lassen Peak, California. Journal of Petrology, **40:** 105-132 (1999).
18. Coombs, M. L., Eichelberger, J. C. and Rutherford, M. J. Experimental and textural constraints on mafic enclave formation in volcanic rocks. Journal of Volcanology and Geothermal Research, **119:** 125-144 (2002).
19. Couch, S., Sparks, R. S. J. and Carrol, R. Mineral disequilibrium in lavas explained by convective self-mixing in open magma chambers. Nature, **411:** 1037-1039 (2001).
20. Daval, D. Petrogenesis of orthopyroxene-magnetite-ilmenite intergrowths from an ultramafic layer. Contributions to Mineralogy and Petrology, **95:** 301-310 (1987).
21. Dimittijevic, M. D. Geology of Kerman region. Geological Survey of Iran, Report Yu/53, 334 p. (1973).
22. Eichelberger, J. C., Gooley, R., Nitsan, U. and Rice, A. A mixing model for andesite volcanism (abstract). EOS Transactions of American Geophysical Union, **57:** 1024 (1976).
23. Eichelberger, J. C. Andesite volcanism and crustal evolution. Nature, **275:** 21-27 (1978).
24. Eichelberger, J. C. Vesiculation of mafic magma during replenishment of silicic magma chambers. Nature, **288:** 446-450 (1980).
25. Eichelberger, J. C., Izbekov, P. E. and Brown, B. L. Bulk chemical trends at arc volcanoes are not liquid lines of descent. Lithos, **87:** 135-154 (2006).
26. Forster, H., Fesefeldt, K. and Kursten, M. Magmatic and orogenic evolution of the Central Iranian volcanic belt. 24th International Geological Congress Science, **2:** 198-210 (1972).
27. Geschwind, C. H. and Rutherford, M. J. Crystallization of microlites during magma ascent: the fluid mechanics of 1980-1986 eruptions at Mount St. Helens. Bulletin of Volcanology, **57:** 356-370 (1995).
28. Gill, J. B. Orogeneic andesites and plate tectonics. Berlin: Springer-Verlag, 390 p. (1981).
29. Ginibre, C., Worner, G. and Kronz, A. Minor- and trace-element zoning in plagioclase: implications for magma chamber processes at Parinacota volcano, northern Chile. Contributions to Mineralogy and Petrology, **143:** 300-315 (2002).
30. Gioncada, A., Mazzuoli, R. and Milton. A. Magma mixing at Lipari (Aeolian Islands, Italy): insights from textural and compositional features of phenocrysts. Journal of Volcanology and Geothermal Research, **145:** 97-118 (2005).
31. Halsor, S. P. Large glass inclusions in plagioclase phenocrysts and their bearing on the origin of mixed andesitic lavas at Toliman Volcano, Guatemala. Bulletin of Volcanology, **51:** 271-280 (1989).
32. Halsor, S. P. and Rose, W. I. Mineralogical relations and magma mixing in calc-andesites from Lake Atitlan, Gutemala. Mineralogy and Petrology, **45:** 47-67 (1991).
33. Hasleton, J. D. and Nash, W. P. Ilmenite-orthopyroxene intergrowths from the moon and the Skaergaard intrusion. Earth Planetary Science Letters, **26:** 287-291 (1975).
34. Humphreys, M. C, S., Blundy, J. D. and Sparks, R. S. J. Magma evolution and open-system processes at Shiveluch Volcano: insights from phenocryst zoning. Journal of Petrology, **47:** 2303-2334 (2006).
35. Jung, D., Kursten, M. and Tarkian, M. Post-Mesozoic volcanism in Iran and its relation to the subduction of the afro-Arabian under the Eurasian plate. In: Pilger, A., Rosler, A., (Eds) Afar between continental and oceanic rifting. Schweiz Verlag lung Stuttgart, pp. 175-181 (1976).
36. Konishi, H. and Akai, J. A transmission electron microscopic study of dusty plagioclase in calc-alkaline andesite from the Oze-Hiuchigatake volcano, central Japan. Mineralogy and Petrology, **53:** 173-187 (1995).
37. Kawamoto, T. Dusty and honeycomb plagioclase; indicator of processes in the Uchino stratified magma chamber, Isu Peninsula, Japan. Journal of Volcanology and Geothermal Research, **49:** 191-208 (1992).
38. Kent, A. R., Darr, C. D., Koleszar, A. M., Salisbury, M. J. and Cooper, K. M., Preferential eruption of andesitic magmas through recharge filtering. Nature Geoscience, **3:** 631-636 (2010).
39. Koyaguchi, T. Textural and compositional evidence for magma mixing and its mechanism, Abu volcano group southwestern Japan. Contributions to Mineralogy and Petrology, **93:** 33-45 (1986).
40. Koyaguchi, T. and Blake, S. Origin of mafic enclaves; constraints on the magma mixing model from fluid dynamic experiments. Enclaves and granite petrology. Development in Petrology, **13:** 415-429 (1991).
41. Le Maitre, R. W. Igneous rocks: A classification and Glossary of Terms: Recommendations of the International Union of Geological Sciences Subcommission on the Systematics of igneous Rocks. Cambridge University Press, Cambridge, 236 p. (2004).
42. Leturmy, P. and Robin, C. Tectonic and stratigraphic evolution of Zagros and Makran during the Mesozoic–Cenozoic: introduction. Geological Society of London Special Publications, **330:** 1-4 (2010).
43. Martin, V. M., Holness, M. B. and Pyle, D. M. Textural analysis of magmatic enclaves from the Kameni Islands, Santorini, Greec. Journal of Volcanology and Geothermal Research, **154:** 89-102 (2006).
44. Morimoto, N., Fabries, J., Ferguson, A. K., Ginzburg, I. V., Ross, M., Seifert, F., Zussman, J., Aoki, K. and Gottardi, G. Nomenclature of pyroxenes. American Mineralogist, **73:** 1123-1133 (1988).
45. Morrice, M. G. and Gill, G. B. Spatial patterns in the mineralogy of island arc magma series: Sangihe Indonesia arc. Journal of Volcanology and Geothermal Research, **29:** 311-353 (1986).
46. Murphy, M. D., Sparks, R. S. J., Barclay, J., Carroll, M. R. and Brewer, T. S. Remobilization of andesite magma by intrusion of mafic magma at the Soufriere Hills Volcano, Montserrat, West Indies. Journal of Petrology, **41:** 21-42 (2000).
47. Ohba, T., Kimura, Y. and Fujimaki, H. High-magnesian andesite produced by two-stage magma mixing: a case study from Hachimantai, Northern Hanshu. Journal of Petrology, **48:** 627-465 (2007).
48. Ownby, S. E., Lange, R. A., Hall, C. M. and Delgado-Granados, H. Origin of andesite in the deep crust and eruption rates in the Tancitaro-Nuvea Italia origin of the central Mexican arc. Geological Society of America Bulletin, **123:** 274-294 (2011).

49. Perugini, D., Valentini, L. and Poli, G. Insights into magma chamber processes from the analysis of size distribution of enclaves in lava flows: A case study from Vulcano Island (Southern Italy). Journal of Volcanology and Geothermal Research, **166:** 193-203 (2007).
50. Pal, T., Mitra, S. K., Sengupta, S., Katari, A., Bandopadhyay, P. C. and Bhattacharya, A. K. Dacite-andesites of Narcondam volcano in the Andaman Sea- An imprint of magma mixing in the inner arc of the Andaman-Java subduction system. Journal of Volcanology and Geothermal Research, **168:** 93-113 (2007).
51. Price, R. C., Gamble, J. A., Smith, I. E. M., Stewart, R. B., Eggins, S. and Wright, I. C. An integrated model for the temporal evolution of andesites and rhyolites and crustal development in New Zealand's north island. Journal of Volcanology and Geothermal Research, **140:** 1-24 (2005).
52. Reubi, O. and Blundy, J. A dearth of intermediate melts at subduction zone volcanoes and the petrogenesis of arc andesite. Nature**, 461:** 1269-1274 (2009).
53. Rudnick, R. L. Making continental crust. Nature, **378:** 571-578 (1995).
54. Sakuyama, M. Petrological study of the Myoko and Kurochime volcanoes, Japan: crystallization sequence and evidence for magma mixing. Journal of Petrology, **22:** 553-583 (1981).
55. Schroder, J. W. Essai sur la structure de I'lran. Eclogae Geologicae Helvetiae, **37:** 37-81 (1944).
56. Sengor, A. M, C. A new modal for the late Paleozoic-Mesozoic tectonic evolution of Iran and implication for Oman. In: Roberson, A.H.F., Srarle, M., Ries, A.C., (Eds) The Geology and Tectonics of the oman region. Geological Society of London Special Publication, **22:** 278-281 (1990).
57. Shahabpour, J. Island-arc affinity of the Central Iranian Volcanic Belt. Journal of Asian Earth Sciences, **30:** 652-665 (2007).
58. Shcherbakov, V. D., Plechov, P. Y., Izbekov, P .E. and Shipman, J. S, Plagioclase zoning as indicator of magma processes at Bezymianny volcano, Kamchatka. Contributions to Mineralogy and Petrology, doi:10.1007 /s00410-010-0584-1: 1-17 (2010).
59. Sparks, R. S. J. and Marshall, L. Thermal and mechanical constraints on mixing between mafic and silicic magmas (Scotland). Journal of Volcanology and Geothermal Research, **29:** 99-124 (1986).
60. Sparks, R. S. J., Folkes, C. B., Humpherys, M. C. S., Barfod, D. N., Lavero, J., Sunagua, M. C. and McNutt, S. R. Uturnch volcano, Bolivia: volcanic unrest due to mid-crust magma intrusion. American Journal of Science, **308:** 727-769 (2008).
61. Sparks, R. S. J., Sigurdsson, H. and Wilson, L. Magma mixiong: a mechanism for triggering acid explosive eruptions. Nature, **267:** 315-318 (1977).
62. Srdic, A., Dimitrijevic, M. N., Cvetic, S. and Dimitrijevic, M. D. Geological Map of Iran, 100,000 Series, Sheet 7348, Baft, (1972).
63. Stimac, J. A. and Pearce, T. H. Textural evidence of mafic-felsic magma interaction in dacite lavas, Clarke Lake, California. American Mineralogist, **77:** 795-809 (1992).
64. Stimac, J.A., Pearce, T. H., Donnely-Nolan, J. M. and Hearn, J. R. B. C. The origin and implications of undercooled andesitic inclusions in rhyolites, Clear Lake volcanics, California. Journal of Geophyical Research, **95:** 17729-17746 (1990).
65. Stockline, J. Structural history and tectonic of Iran. Bulletin of American Association of Petroleum Geologists, **52:** 1229-1258 (1968).
66. Tatsumi, Y., Takahashi, T., Hirahara, Y., Chang, Q., Miyazaki, T., Kimura, J. I., Ban, M. and Sakayori. A. New insights into andesite genesis: the role of mantle-derived calc-alkalic and crust-derived tholeiitic melts in magma differentiation beneath Zao Volcano, NE Japan. Journal of Petrology, **49:** 1971-2008 (2008).
67. Toscani, L., Venturelli, G., Barbieri, M., Capedri, S., Fernandez Soler, J. M. and Oddone, M. Geochemistry and petrogenesis of two-pyroxene andesites from Sierra de Gata (SE Spain). Mineralogy and Petrology, **41:** 199-213 (1990).
68. Tsuchiyama, A. Dissolution kinetics of plagioclase in the melt of the system diopside-albite-anorthite, and origin of dusty plagioclase in andesite. Contributions to Mineralogy and Petrology, **89:** 1-16 (1985).
69. Tsune, A. and Toramaru, A. A simple model of oscillatory zoning in magmatic plagioclase: development of an isothermal undercooling model. American Mineralogist, **92:** 1071–1079 (2007).